

PAPER • OPEN ACCESS

## The Effect of Heat Treatment on the Microstructure of $\text{Co}_{50}\text{Ni}_{25}\text{Al}_8\text{Ti}_8\text{Nb}_3\text{Ta}_3\text{W}_3$ High Entropy Alloy and Its High-temperature Oxidation Resistance

To cite this article: Chaojie Liang *et al* 2021 *J. Phys.: Conf. Ser.* **2044** 012069

View the [article online](#) for updates and enhancements.

You may also like

- [Microstructures and shape memory characteristics of Ti-25Ni-25Cu\(at.%\) alloy ribbons](#)  
Tae-hyun Nam, Soo-moon Park, Tae-yeon Kim *et al.*
- [Mechanical and functional properties of amorphous-crystalline thin ribbons of  \$\text{Ti}\_{50}\text{Ni}\_{25}\text{Cu}\_{25}\$  and  \$\text{Ti}\_{40.7}\text{Hf}\_{9.3}\text{Ni}\_{44.8}\text{Cu}\_5\$  shape memory alloys](#)  
S Belyaev, N Resnina and V Slesarenko
- [Fabrication of Three-Dimensional Nanoporous Nickel by Dealloying Mg-Ni-Y Metallic Glasses in Citric Acid Solutions for High-Performance Energy Storage](#)  
Lei Zuo, Ran Li, Yu Jin *et al.*



**ECS**  
The  
Electrochemical  
Society  
Advancing solid state &  
electrochemical science & technology

**DISCOVER**  
how sustainability  
intersects with  
electrochemistry & solid  
state science research

# The Effect of Heat Treatment on the Microstructure of $\text{Co}_{50}\text{Ni}_{25}\text{Al}_8\text{Ti}_8\text{Nb}_3\text{Ta}_3\text{W}_3$ High Entropy Alloy and Its High-temperature Oxidation Resistance

Chaojie Liang<sup>1,a</sup>, Chenglei Wang<sup>1,b\*</sup>, Kexiang Zhang<sup>1</sup>, Hong Tan<sup>2</sup>, Mulin Liang<sup>1</sup>, Yingguang Xie<sup>1</sup>, Weijie Liu<sup>1</sup>, Jijie Yang<sup>1</sup>, Shengfeng Zhou<sup>3</sup>

<sup>1</sup> Guangxi Key Laboratory of Information Materials and School of Materials Science and Engineering, Guilin University of Electronic Technology, Guilin 541004, P.R. China

<sup>2</sup> Guilin Medical University, Guilin, 541001, P.R. China

<sup>3</sup> Institute of advanced wear & corrosion resistance and functional materials, Jinan university, Guangdong, Guangzhou 510632, P.R. China

<sup>a</sup> e-mail: cj11274@163.com.

\* Corresponding author: e-mail: wangxuelel@guet.edu.cn.

**Abstract:** The design based on high-entropy alloys (HEAs) is undergoing a conceptual expansion from equiatomic alloys to non-equiatomic alloys. To provide the experimental basis for non-equiatomic high-entropy alloys and their oxidation resistance at high temperatures, in this study, a  $\text{Co}_{50}\text{Ni}_{25}\text{Al}_8\text{Ti}_8\text{Nb}_3\text{Ta}_3\text{W}_3$  high-entropy alloy was prepared by a vacuum arc melting method, and then it was subjected to different aging heat treatments. The phase composition, element composition distribution, and mechanical properties of the alloy were characterized by XRD, SEM/EDS. In addition, we have systematically studied the high-temperature oxidation resistance of the alloy and analyzed the high-temperature oxidation mechanism of the alloy. The results showed that the phase composition of the  $\text{Co}_{50}\text{Ni}_{25}\text{Al}_8\text{Ti}_8\text{Nb}_3\text{Ta}_3\text{W}_3$  high-entropy alloy is a single fcc solid solution phase, and the grains of the alloy become coarser after secondary aging. Many oxidation products were produced after high-temperature oxidation of the alloy. The oxidation products of the outermost layer of the alloy are mainly  $\text{CoNiO}_2$ ,  $\text{CoTiO}_3$ , and  $\text{Ni}_2\text{O}_3$ , and the oxidation products of the intermediate layer are mainly  $\text{Al}_2\text{O}_3$ ,  $\text{TiO}_2$ , and  $\text{Nb}_2\text{O}_3$ .

## 1. Introduction

The conventional alloys are composed of one or two elements, in these conventional alloys, few minor elements are incorporated into the matrix of the principal element to enhance the properties. With the development of society, the demand for the properties of alloys has further increased, and traditional alloy design concepts can no longer meet the current demand for alloy properties. This conventional alloy design strategy has been altered considerably to lead to the discovery of a new class of alloys, known as multi-principal alloy or high-entropy alloys (HEAs) have proposed by Yeh and Cantor in 2004<sup>[1,2]</sup>. This alloy design concept is a new attempt in the field of metals. It is a new type of alloy design through the configuration entropy between elements. HEAs are defined hence to consist of four principal alloying elements, and the molar concentration of each element is between 5 at.%- 35 at.%. Interestingly, it was confirmed that this kind of alloy with multi-principal elements tends to a form simple solid-



solution structure rather than complex phases or intermetallic compounds due to the high configurational entropy of the alloys [3-5]. For example, CoCrFeMnNi [6] and AlCuFeCrNi [7] high-entropy alloys can form a simple fcc solid solution structure. CuMoTaWV [8] and NbMoTaWVZr [9] can form a simple bcc structure. HEAs have many excellent properties, such as good thermal stability, high strength, high hardness, excellent corrosion resistance, and friction and wear resistance, as well as good magnetic properties and high-temperature oxidation resistance [10-20]. The applications of HEAs are diverse due to the diversity of properties of HEAs, and it means that HEAs have a great potential for application.

Refractory high-entropy alloys (RHEAs) [21] composed of alloying elements with high melting points have excellent high-temperature strength. Since their first emergence, RHEAs have been considered as potential next-generation high-temperature materials that can break the temperature limits of current alloys, such as nickel-based Superalloys [22]. In recent years, RHEAs have attracted more and more attention from researchers due to their inherent high-temperature strength and excellent resistance to high-temperature softening [23]. However, despite the many advantages of RHEAs, it suffers from room temperature brittleness and insufficient oxidation resistance. In contrast, many studies have proved that the room temperature brittleness of RHEAs can be achieved through electronic theory [24] or phase transformation [25] to achieve a trade-off between ductility and plasticity. How to improve the oxidation resistance of RHEAs is a more urgent problem to be solved. Most of the RHEAs reported in the literature are prone to catastrophic oxidation via internal oxidation of the alloy when exposed to high temperatures [26,27].

Oxidation resistance is very important for high-temperature applications to structural alloys because the formation of oxides can lead to a severe decrease in mechanical properties or catastrophic failure. From the traditional perspective of alloy design, the main strategy to improve the oxidation resistance is to infiltrate Al, Cr, or Si element, because these elements are expected to form a stable and dense oxide layer (such as Al<sub>2</sub>O<sub>3</sub>, Cr<sub>2</sub>O<sub>3</sub>, and SiO<sub>2</sub>), which can effectively prevent further oxidation due to hinder the O<sup>2-</sup> into the alloy interior [28-30].

Taking into account the typical "cocktail effect" in high-entropy alloys, Co, Ni, Nb, Ta, W, and Al elements are considered for this study to carry out the alloy design, it is due to Co, Ni, Nb, Ta, and W elements have good high-temperature performance, and Al element has good oxidation resistance. And it is worth to note that the high solubility of Ta and W in the alloy can reduce the stacking fault energy in the matrix, increase the number and temperature of precipitated phase in the alloy, refine the size of precipitated phase particles, and increase the stability of its long-term aging. Nb can increase the amount of precipitated phase, refine the grain and improve the mechanical properties of the alloy. Al, Ti, and Nb are the main precipitation strengthening elements of the alloy, which can increase the initial melting temperature of the alloy, expand the temperature range of solid solution treatment of the alloy, facilitate the heat treatment and uniform precipitation of precipitated phase, reduce the kinetics of precipitation coarsening, form cluster structure in the matrix phase, hinder the dislocation movement, and improve the high temperature performance of the alloy.

It is known that heat treatment can lead to the structural transformation of the alloy, so different types of heat treatment on the alloy are also considered in this study. In this study, we have studied the effect of heat treatment on the structural transformation and mechanical properties of the alloy. In addition, we also tested its oxidation resistance at high-temperature and analyzed its oxidation kinetics, hope to provide an experimental reference for the study of HEAs at high temperatures.

## 2. Experimental procedures

Co, Ni, Al, Ti, Nb, Ta, and W metals with purity no less than 99.9% wt.% were used to prepare Co<sub>50</sub>Ni<sub>25</sub>Al<sub>8</sub>Ti<sub>8</sub>Nb<sub>3</sub>Ta<sub>3</sub>W<sub>3</sub> (in the atomic ratio) HEAs. Before smelting, the vacuum in the smelting furnace should be pumped below  $3.0 \times 10^{-3}$  Pa, and then high-purity argon gas is passed in to make the pressure in the furnace around 0.5 Pa. And then the alloy was melted in a high-purity argon atmosphere by vacuum arc melting with a water-cooled copper mold. The ingots were remelted at least five times to ensure chemical homogeneity. To study the influence of the aging process on the structure and properties of the alloy, the alloy was isothermally homogenized at 1200°C for 4h firstly and then

subjected to different aging treatments. Finally, the alloys were subjected to water quenching and prepared to detect. The aging process of the alloy is shown in Table 1.

The crystal structure was analyzed with the Germany Bruker D8 Advance X-ray diffractometer using Cu K $\alpha$  radiation scanning from 10°C to 90°C at a rate of 10°C/min. The observation of microstructures and the phase compositions of the alloy via scanning electron microscope (SEM, Quanta 450) equipped with an energy dispersive spectrometer (EDS). HV-1000 micro-hardness tester was used to test the hardness of the alloy. The high-temperature oxidation resistance test was carried out in a 900°C air atmosphere with a box-type resistance furnace, and a single sample was cyclically oxidized. Before the oxidation test, the surface of the sample was ground with 2000#, followed by a polish with 1.5 $\mu$ m diamond paste and ultrasonic cleaning in acetone, using the discontinuous weighing method to measure the oxidative weight gain of the sample, and the cross-sectional morphology and composition of the sample after the oxidative weight gain were analyzed by XRD, SEM, and EDS.

Table.1 Heat treatment process of alloy

Number	Type
H1	800 °C×24 h
H2	1000 °C×4 h+800 °C×24 h
H3	1000 °C×4 h+900 °C×24 h

### 3. Results and discussion

The X-ray patterns of the alloy are presented in Fig.1, and the atomic radius of each element list in Table.2. The alloy still has the same characteristic diffraction peaks after different types of heat treatment, and no other diffraction peaks of complex phases are found. This is because the multi-principal element alloy has a high mixing entropy effect, and the atoms between the principal elements have a strong cooperative diffusion effect, thereby inhibiting the formation of intermetallic compounds and promoting the formation of a simple solid solution structure. The alloy is directly aged after solution treatment at 1200°C, the peak intensity is the highest, while the peak intensity of the secondary aging alloy is significantly reduced. Also, the highest fcc peak has a small angle shift to the left which can be seen from the inset pattern. That's because the structure of the alloy is coarser than that under the primary aging heat treatment after the secondary aging heat treatment of the alloy, causing the XRD peak intensity of the alloy to be weakened and shifted. Besides, the lattice distortion of the alloy is increased after the secondary aging heat treatment of the alloy. From the Bragg diffraction law, the lattice constant of the alloy becomes larger, so the XRD peak intensity of the alloy shifts to the left. According to the Bragg equation:

$$2d \sin \theta = n\lambda \quad (1)$$

Where  $d$  is the spacing of crystal planes,  $\theta$  is the incident angle,  $\lambda$  is the wavelength of the X-ray, which is a fixed value. From the Bragg diffraction law (formula 1), the lattice constant of the alloy becomes larger, so the XRD peak intensity of the alloy shifts to the left. The increase of the aging temperature will also cause the XRD peak to shift to the left under the same aging method. This is because the increase in temperature causes the alloy grains to be coarser. It is worth noting that after the secondary aging heat treatment, a new fcc peak is detected near 73°, which indicates that the alloy has formed a new fcc structure phase after the secondary aging heat treatment.

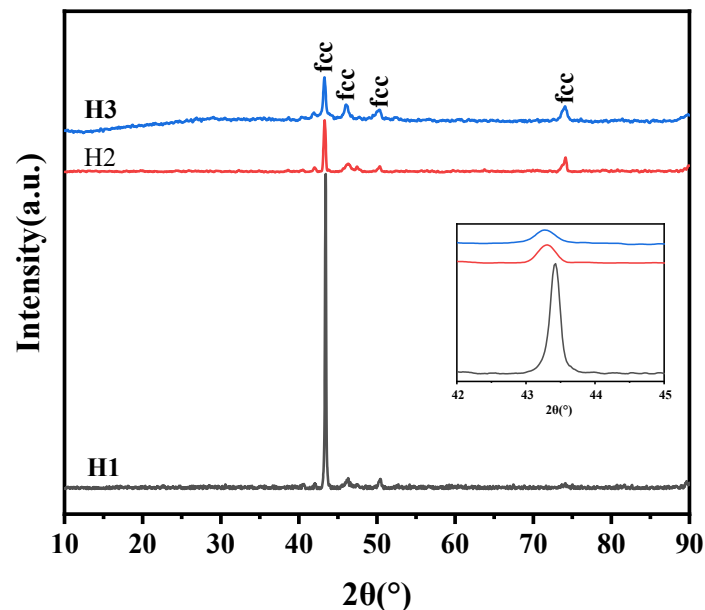


Fig.1 XRD analysis on alloys after different heat treatment

The microstructure of the alloys examined with SEM is shown in Fig.2. The structure of the alloys is dendritic and interdendritic. The structure of the alloys under different aging heat treatment methods is different, which shows that the aging treatment method has a greater influence on the structure. The structure of the alloy after two-stage aging is larger than that of the single-stage aging alloy. And under the same aging method, the increase in temperature will also cause the coarsening of the alloy structure. At the same time, it is shown that when the final aging temperature and time are the same, the grains of the alloy will be coarser after the secondary aging, and the secondary aging is not conducive to grain refinement.

Table.2 gives the EDS analysis results and hardness values of the alloys. The content of Co and Ni in the dendrite and dendrite is similar, the distribution is relatively uniform, and there is no segregation phenomenon, Al and W are enriched in dendrites, Ti, Nb, and Ta are enriched in dendrites, as shown in Table.2. That's because Al and W have relatively negative mixing enthalpies with other elements while mixing enthalpies of Ti, Nb, and Ta is relatively large, as shown in Table.3. The presence of Al and W will severely hinder the existence of Ti, Nb, and Ta in the dendrites, and push the Ti, Nb, and Ta elements into the dendrite. Besides, with the change of aging method and aging temperature, the hardness value of the alloy changes significantly. When the final aging temperature is 800°C, the hardness value of the alloy decreases from 342HV to 310HV, the rate of decrease is 9.4%. When the final aging temperature rises from 800°C to 900°C, the hardness value of the alloy decreases from 310HV to 265HV, the rate of decrease is 14.5%. It can be summarized that with the change of the aging method and the increase of the aging temperature, the structure of the alloys becomes coarser, which leads to the decrease of the hardness of the alloy.

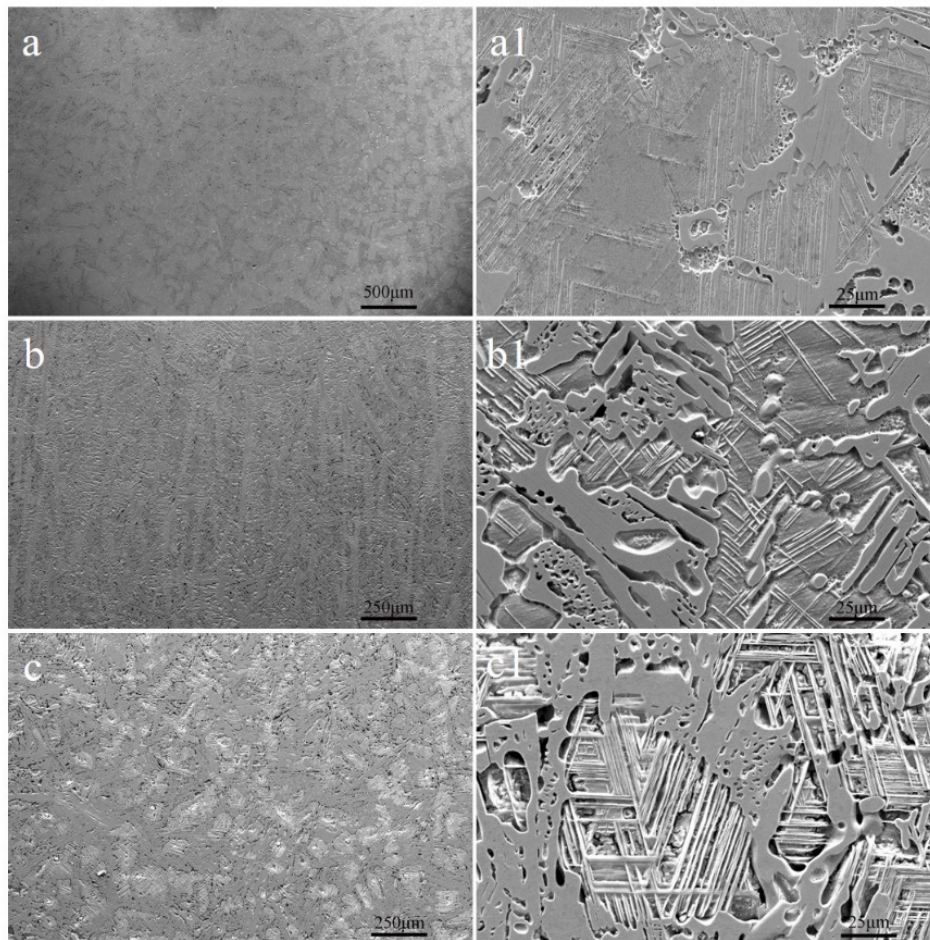


Fig.2 The SEM image of the alloys (a)H1; (b)H2; (c)H3

Table.2 The hardness, chemical composition (at. %) of the alloys

Alloys	Hardness (HV)	Region	Co (1.26Å)	Ni (1.24Å)	Al (1.43Å)	Ti (1.45Å)	Nb (1.48Å)	Ta (1.48Å)	W (1.41Å)
H1	342± 5	ID	50.90	23.35	5.32	8.97	3.84	3.79	3.84
		DR	49.19	24.72	8.43	7.95	2.01	3.09	4.62
H2	310± 10	ID	49.20	25.10	5.60	8.87	4.23	3.75	3.25
		DR	50.50	24.24	7.88	8.19	2.22	3.19	3.78
H3	265± 8	ID	50.57	23.62	5.29	8.82	3.84	3.88	3.99
		DR	46.02	23.04	6.64	10.14	3.50	4.28	6.38

Table.3 Mixing enthalpies (KJ/mol) of atomic pairs between elements <sup>[22]</sup>

	Co	Ni	Al	Ti	Nb	Ta	W
Co	-	0	-19	-28	-25	-24	-1
Ni	-	-	-22	-35	-30	-30	-3
Al	-	-	-	-30	-18	-19	-2
Ti	-	-	-	-	2	1	-6
Nb	-	-	-	-	-	0	-8
Ta	-	-	-	-	-	-	-7
W	-	-	-	-	-	-	-

The mass gain versus time plots can be modeled by the oxide growth law, using the equation <sup>[31,32]</sup>:

$$\Delta m = (k_p t)^n \quad (2)$$

Where  $\Delta m$  is the specific mass gain,  $K_p$  is oxide growth rate constant,  $t$  is the oxidation time, and  $n$  is the time exponent which can be fixed to 0.5 for a typical parabolic oxidation behavior <sup>[33]</sup>. The  $K_p$  value of the alloy in this study is calculated by the formula (2) to be  $1.6 \times 10^{-2} \text{ mg}^2 \cdot \text{cm}^{-4} \cdot \text{h}^{-1}$ . It is worth noting that the high-temperature oxidation resistance test under the same conditions found that the alloy in this study has good oxidation resistance, as shown in Table 4. The mass gain versus time plots of the alloy after oxidation at 900°C in the air for 55h is shown in Fig.3(a). The mass gain versus time plots of the alloy conforms to the parabolic law. The high-temperature oxidation weight gain of the alloy increases with the extension of the oxidation time. The alloy has a large increase in weight during the first 8 hours of oxidation. When the alloy is oxidized at 900°C for 10 to 55 h, the oxidation weight gain of the alloy tends to be andante, as shown in Fig.3(a). No peeling of the oxide layer on the surface of the alloy was observed during the weight gain process, indicating that the formed oxide layer has a good bonding force with the base alloy.

Fig.3(b) depicts the XRD pattern of the alloy surface after oxidized in air at 900°C for 55h. Many oxidation products are produced after high-temperature oxidation of the alloy, which are  $\text{Al}_2\text{O}_3$ ,  $\text{TiO}_2$ ,  $\text{Nb}_2\text{O}_3$ ,  $\text{Ni}_2\text{O}_3$ ,  $\text{CoNiO}_2$ , and  $\text{CoTiO}_3$ . Fig.3(c) is the cross-sectional morphology and EDS analysis results of the alloy after being oxidized in air at 900°C for 55h. The oxide layer formed in the alloy is thicker, about 30 $\mu\text{m}$ . Combined with the previous XRD analysis, the oxidation products of the outermost layer of the alloy are mainly  $\text{CoNiO}_2$ ,  $\text{CoTiO}_3$ , and  $\text{Ni}_2\text{O}_3$ . The oxidation products of the intermediate layer between the base alloy and the outermost oxide film are mainly  $\text{Al}_2\text{O}_3$ ,  $\text{TiO}_2$ , and  $\text{Nb}_2\text{O}_3$ . Besides, the oxidation product  $\text{Al}_2\text{O}_3$  is mainly distributed in the intermediate layer, which indicates that during the high-temperature oxidation process, the  $\text{Al}_2\text{O}_3$  formed can effectively prevent the further diffusion of  $\text{O}^{2-}$  into the alloy interior, thereby increasing the high-temperature antioxidant properties of the alloy. Secondly, the oxidation products  $\text{CoNiO}_2$ ,  $\text{CoTiO}_3$ , and  $\text{Ni}_2\text{O}_3$  are produced in the outermost layer, and the oxidation products  $\text{TiO}_2$  and  $\text{Nb}_2\text{O}_3$  are produced in the intermediate layer are very dense. As the oxidation time increases, the O concentration of these two oxide layers continues to increase, causes the brittleness of the oxide layer to increase, so the oxide layer will produce obvious delamination and cracks.

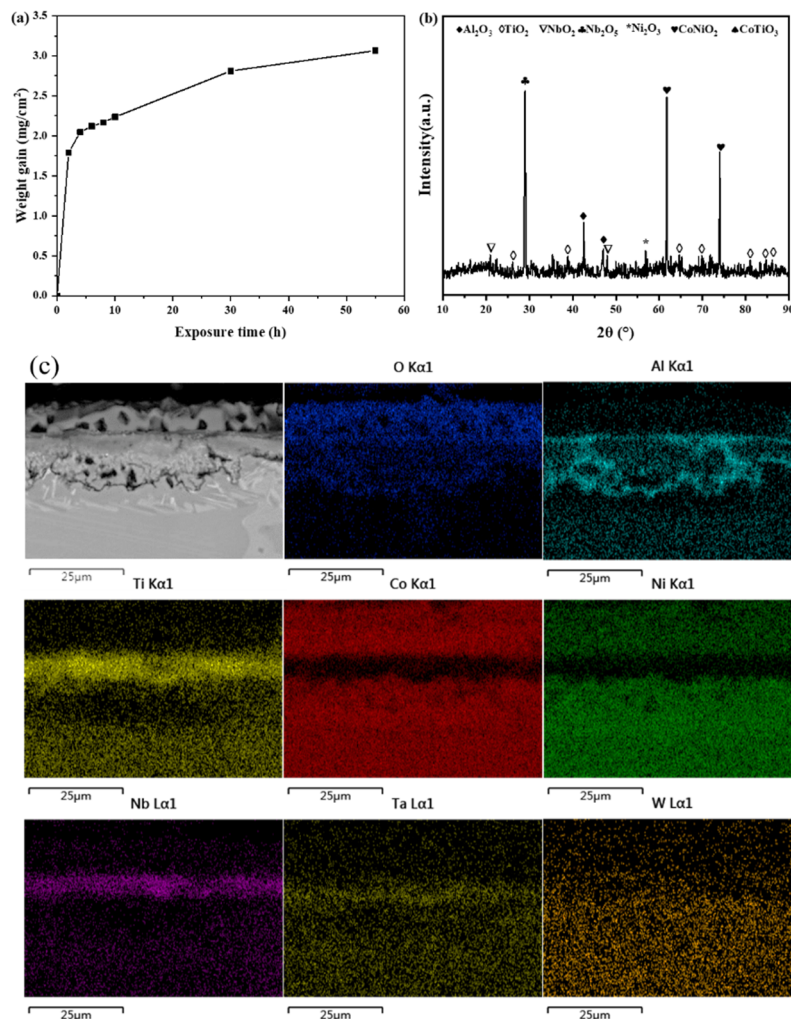


Fig.3 (a) Specific mass change versus time plots for the alloy at 900 °C, (b) XRD pattern of the alloy oxidation in air, and (c) SEM and EDS mapping of the cross-section of the alloy after 900 °C/55h oxidation in air

Table.4 The parabolic constant of the alloy

Alloys	$k_p$ ( $\text{mg}^2 \cdot \text{cm}^{-4} \cdot \text{h}^{-1}$ )	Oxidation method	References
	900 °C		
CoNiAlTiNbTaW	$1.6 \times 10^{-2}$	Box Furnace	Present study
CoCrNi	$4.39 \times 10^{-2}$	Box Furnace	[34]
CoCrFeMnNi	$1.80 \times 10^{-2}$	Box Furnace	[35]
SS 304	6.04	Box Furnace	[36]
CrMnFeCoNi	0.13	Box Furnace	[37]
CrMnFeCoNi	0.1487	Box Furnace	[37]

**4. Conclusions**

The  $\text{Co}_{50}\text{Ni}_{25}\text{Al}_8\text{Ti}_8\text{Nb}_3\text{Ta}_3\text{W}_3$  high-entropy alloy was prepared by vacuum arc melting. The phase composition, the microstructure of the alloy before and after high-temperature oxidation of the alloy were observed and analyzed by XRD, SEM, and EDS, and the following conclusions can be drawn:

(1)  $\text{Co}_{50}\text{Ni}_{25}\text{Al}_8\text{Ti}_8\text{Nb}_3\text{Ta}_3\text{W}_3$  high-entropy alloy has a dendritic structure. The structure of the alloy is different via different aging heat treatment methods, and the aging treatment method has a greater impact on the structural transformation of the alloy. The increase in temperature will cause the coarser

structure of the alloy under the same aging method. At the same time, when the final aging temperature and time are the same, the grains of the alloy will be coarser after the secondary aging, and the secondary aging is not conducive to grain refinement.

(2) The EDS analysis shows that the Co and Ni elements in the  $\text{Co}_{50}\text{Ni}_{25}\text{Al}_8\text{Ti}_8\text{Nb}_3\text{Ta}_3\text{W}_3$  high-entropy alloy are uniformly distributed without segregation, Al and W are concentrated in the dendrites, Ti, Nb, and Ta are concentrated in the interdendritic.

(3) With the change of the aging method and aging temperature, the hardness value of the alloy changes significantly. The hardness value of the alloy after two-stage aging is lower than that of single-stage aging.

(4) Many oxidation products are produced after high-temperature oxidation of the alloy. The oxidation products of the outermost layer of the alloy are mainly  $\text{CoNiO}_2$ ,  $\text{CoTiO}_3$ , and  $\text{Ni}_2\text{O}_3$ , the oxidation products of the intermediate layer are mainly  $\text{Al}_2\text{O}_3$ ,  $\text{TiO}_2$ , and  $\text{Nb}_2\text{O}_3$ .

(5) The oxidation kinetic curve of the alloy conforms to the parabolic law. The  $K_p$  value of the alloy in this study is  $1.6 \times 10^{-2} \text{ mg}^2 \cdot \text{cm}^{-4} \cdot \text{h}^{-1}$ , and the alloy has good high-temperature oxidation resistance.

### Acknowledgments

The authors wish to thank the Natural Science Foundation of Guangxi Province (2018GXNSFAA281244 and 2020GXNSFAA297060), China Postdoctoral Science Foundation Funded Project (2020M681092), the Projects of MOE Key Lab of Disaster Forecast and Control in Engineering in Jinan University (20200904006), and Guangdong Basic and Applied Basic Research Foundation (2020B15150004), Scientific Research and Technology Development Program of Guilin (2020010903), Engineering Research Center of Electronic Information Materials and Devices, Ministry of Education (EIMD-AB202009), Guangxi Key Laboratory of Information Materials (171019-Z, 191006-Z, and 201016-Z), and Innovation Project of GUET Graduate Education (2020YCXS118) for the financial support given to this work.

### References

- [1] J.W. Yeh, S.K. Chen, S.J. Lin, et al. Nanostructured high-entropy alloys with multiple principal elements: novel alloy design concepts and outcomes, *Adv. Eng. Mater.* 6 (2004) 299-303.
- [2] B. Cantor, I.T.H. Chang, P. Knight, et al. Microstructural development in equiatomic multicomponent alloys, *Mater. Sci. Eng. A.* 375 (2004) 213–218.
- [3] Y. Tong, J.C. Qiao, Y. Yao. The constitutive model and threshold stress for characterizing the deformation mechanism of  $\text{Al}_{0.3}\text{CoCrFeNi}$  high entropy alloy, *Mater. Sci. Eng. A.* 730 (2018) 137-146.
- [4] A. Verma, P. Tarete, A.C. Abhyankar, et al. High temperature wear in  $\text{CoCrFeNiCu}_x$  high entropy alloys: The role of Cu, *Scripta Mater.* 161 (2019) 28-31.
- [5] Y. Yu, F. He, Z.H. Qiao, et al. Effects of temperature and microstructure on the tribological properties of  $\text{CoCrFeNiNb}_x$  eutectic high entropy alloys, *J. Alloys Comd.* 775 (2019) 1376-1385.
- [6] F. Otto, A. Dlouhy, C. Somsen, et al. The influences of temperature and microstructure on the tensile properties of a  $\text{CoCrFeMnNi}$  high-entropy alloy, *Acta Mater.* 61 (2013) 5743–5755.
- [7] B. Gwalani, D. Choudhuri, V. Soni, et al. Cu assisted stabilization and nucleation of  $\text{L}_{12}$  precipitates in  $\text{Al}_{0.3}\text{CuFeCrNi}_2$  fcc-based high entropy alloy, *Acta Mater.* 129 (2017) 170-182.
- [8] S. Alvi, F. Akhtar. High temperature tribology of  $\text{CuMoTaWV}$  high entropy alloy, *Wear.* 426-427 (2019) 412-419.
- [9] Y. Long, X.B. Liang, K. Su, et al. A fine-grained  $\text{NbMoTaWVCr}$  refractory high-entropy alloy with ultra-high strength: Microstructural evolution and mechanical properties, *J. Alloys Comd.* 780 (2019) 607-617.
- [10] J.W. Yeh. Recent progress in high-entropy alloys, *Ann. Chim. Sci. Des. Mater.* 31 (6) (2006) 633-648.
- [11] Y. Zhang, Y.J. Zhou, J.P. Lin, et al. Solid-solution phase formation rules for multi-component alloys, *Adv. Eng. Mater.* 10 (6) (2008) 534-538.

- [12] S. Singh, N. Wanderka, B.S. Murty, et al. Decomposition in multi-component AlCoCrCuFeNi high-entropy alloy, *Acta Mater.* 59 (1) (2011) 182-190.
- [13] Y. Chen, T. Duval, U. Hung, et al. Microstructure and electrochemical properties of high entropy alloys: a comparison with type-304 stainless steel, *Corros. Sci.* 47 (9) (2005) 2257-2279.
- [14] Y.J. Zhou, Y. Zhang, Y.L. Wang, et al. Solid solution alloys of AlCoCrFeNiTi<sub>x</sub> with excellent room-temperature mechanical properties, *Appl. Phys. Lett.* 90 (18) (2007).
- [15] J.M. Zhu, H.M. Fu, H.F. Zhang, et al. Microstructure and compressive properties of multiprincipal component AlCoCrFeNiC<sub>x</sub> alloys, *J. Alloys Compd.* 509 (8) (2011) 3476-3480.
- [16] O.N. Senkov, G.B. Wilks, D.B. Miracle, et al. Refractory high-entropy alloys, *Intermetallics*. 18 (9) (2010) 1758-1765.
- [17] D.-H. Lee, J.-M. Park, G. Yang, et al. Nano-graining a particle-strengthened high-entropy alloy. *Scripta Mater.* 163 (2019) 24-28,
- [18] M.H. Chuang, M.H. Tsai, W.R. Wang, et al. Microstructure and wear behavior of Al<sub>x</sub>Co<sub>1.5</sub>CrFeNi<sub>1.5</sub>Ti<sub>y</sub> high-entropy alloys, *Acta Mater.* 59 (2011) 6308-6317.
- [19] S.T. Chen, W.Y. Tang, Y.F. Kuo, et al. Microstructure and properties of age-hardenable Al<sub>x</sub>CrFe<sub>1.5</sub>MnNi<sub>0.5</sub> alloys, *Mater. Sci. Eng. A* 527 (2010) 5818-5825.
- [20] C.P. Lee, C.C. Chang, Y.Y. Chen, et al. Effect of the aluminium content of Al<sub>x</sub>CrFe<sub>1.5</sub>MnNi<sub>0.5</sub> high-entropy alloys on the corrosion behaviour in aqueous environments, *Corros. Sci.* 50 (2008) 2053-2060.
- [21] O.N. Senkov, G.B. Wilks, J.M. Scott, et al. Mechanical properties of Nb<sub>25</sub>Mo<sub>25</sub>Ta<sub>25</sub>W<sub>25</sub> and V<sub>20</sub>Nb<sub>20</sub>Mo<sub>20</sub>Ta<sub>20</sub>W<sub>20</sub> refractory high entropy alloys, *Intermetallics*. 19 (5) (2011) 698-706.
- [22] O.N. Senkov, G.B. Wilks, D.B. Miracle, C.P. Chuang, P.K. Liaw, Refractory high-entropy alloys, *Intermetallics* 18 (9) (2010) 1758-1765.
- [23] D.M. Dimiduk, J.H. Perepezko, Mo-Si-B alloys: developing a revolutionary turbine-engine material, *MRS Bull.* 28 (9) (2003) 639-645.
- [24] S. Sheikh, S. Shafeie, Q. Hu, et al, Alloy design for intrinsically ductile refractory high-entropy alloys, *J. Appl. Phys.* 120 (2016) 164902.
- [25] H. Huang, Y. Wu, J. He, et al. Phase-transformation ductilization of brittle high-entropy alloys via metastability engineering, *Adv. Mater.* 29 (30) (2017) 1701678.
- [26] S. Sheikh, L. Gan, T.-K. Tsao, et al. Aluminizing for enhanced oxidation resistance of ductile refractory high-entropy alloys, *Intermetallics*. 103 (2018) 40-51.
- [27] Y.J. Chang, A.C. Yeh. The evolution of microstructures and high temperature properties of Al<sub>x</sub>Co<sub>1.5</sub>CrFeNi<sub>1.5</sub>Ti<sub>y</sub> high entropy alloys, *J. Alloys Comd.* 653 (2015) 379-385.
- [28] A. Takeuchi, A. Inoue. Intermetallics Mixing enthalpy of liquid phase calculated by miedema's scheme and approximated with sub-regular solution model for assessing forming ability of amorphous and glassy alloys, *Intermetallics*. 18 (2010) 1779-1789.
- [29] B. Gorr, F. Mueller, M. Azim, et al, A. Kauffmann, M. Heilmaier, High-temperature oxidation behavior of refractory high-entropy alloys: effect of alloy composition, *Oxid. Metals* 88 (3-4) (2017) 339-349.
- [30] F. Mueller, B. Gorr, H.J. Christ, et al, Effect of microalloying with silicon on high temperature oxidation resistance of novel refractory high-entropy alloy Ta-Mo-Cr-Ti-Al, *Mater. A. T. High. Temp.* 35 (1-3) (2018) 168-176.
- [31] J. Dąbrowa, G. Cieślak, M. Stygar, et al. Influence of Cu content on high temperature oxidation behavior of AlCoCrCu<sub>x</sub>FeNi high entropy alloys (x = 0; 0.5; 1), *Intermetallics*. 84 (2017) 52-61.
- [32] Y.Y. Liu, Z. Chen, Y.Z. Chen, et al. Effect of Al content on high temperature oxidation resistance of Al<sub>x</sub>CoCrCuFeNi high entropy alloys (x=0, 0.5, 1, 1.5, 2), *Vacuum*. 169 (2019).
- [33] N. Birks, G.H. Meier, F.S. Pettit. Introduction to the High Temperature Oxidation of Metals, Cambridge University Press, Cambridge, 2006.
- [34] M.P. Adomako, J.H. Kim, Y.T. Hyun. High-temperature oxidation behaviour of low-entropy alloy to medium- and high-entropy alloys, *J. Therm. Anal. Calorim.* 133 (2018) 13-26.

- [35] M.P. Agustianingrum, U. Lee, N. Park. High-temperature oxidation behaviour of CoCrNi medium-entropy alloy, *Corros. Sci.* 173 (2020) 108755.
- [36] Y.K. Kima, Y.A. Jooa, H.S. Kimb, K.A. Leea, High temperature oxidation behavior of Cr-Mn-Fe-Co-Ni high entropy alloy, *Intermetallics*. 98 (2018) 45-53.
- [37] G. Laplanche, U.F. Volkert, G. Eggeler, E.P. George, Oxidation behavior of the CrMnFeCoNi high-entropy alloy, *Oxid. Met.* 85 (2016) 629–645.